Orbital-selective mixed-valent Mott/metal phase coexistence in NdNiO$_2$ films

Luis Craco[1] and Stefano Leoni [2]

[1]*Institute of Physics, Federal University of Mato Grosso, 78060-900 Cuiabá, Mato Grosso, Brazil*
[2]*School of Chemistry, Cardiff University, Cardiff CF10 3AT, United Kingdom*

A plethora of fundamentally different electronic states can coexist in orbital-selective systems, including Mott-localized, pseudogapped, Fermi, and non-Fermi-liquid phases. Understanding their emergence as a result of electronic correlations remains a fundamental challenge in condensed matter theory. Superconductivity in infinite-layer nickelates is driven by a subtle balance between valence charge and crystal structures, two aspects that are strongly affected by synthetic protocols. Here, using density functional plus dynamical mean-field theory, we explore correlation and hole-doping-induced electronic reconstruction in the NdNiO$_2$ superconductor. Based on a direct comparison with extant RIXS data, we show that the electronic spectra of NdNiO$_2$ films can be understood as mixed valence due to static modulation of $3d^9$/$3d^8$ Mott/metal states. The coexistence of Mott-localized $3d^9$ and partially restored Fermi-liquid $3d^8$ low-energy excitations results in a two-fluid system exhibiting different coupling parameters, a novel scenario in infinite-layer nickelate superconductors. We expect that our present results are also applicable to access novel phases of matter in other quantum systems, in which structural domains can host different doping levels.

I. INTRODUCTION

The search for superconductivity in infinite-layer nickelates [1,2] has introduced an important new family of unconventional superconductors with electrical resistivity $\rho_{dc}(T)$ displaying clear deviations from the conventional T^2 dependence of Fermi liquid (FL) metals [3]. Extensive theoretical studies indicate that orbital degrees of freedom and electronic correlations are relevant in this material class [4–10]. An important question in this field is therefore whether orbital selectivity determines the electronic state that might host unconventional superconductivity [11]. This is of fundamental importance for the nickelate superconducting materials since they are commonly understood in relation to cuprates, both structurally and electronically [4,6,12].

The apical oxygens can in fact be reductively removed from rare-earth perovskite nickelate precursors [13], yielding rare-earth infinite-layer nickelates with quasi-two-dimensional NiO$_2$ planes separated by single layers of rare-earth atoms, which are isostructural to the cuprate oxide superconductors. The analogy between 112 nickelates and CaCuO$_2$ [14] is further underpinned by Cu^{2+} and Ni^{1+} having the same formal $3d^9$ ionic configuration. However, key differences in the multiorbital (MO) nature of the low-energy electronic states [4–10] between cuprates and nickelates suggest more similarities to Fe-chalcogenide superconductors [15] rather than cuprates.

While the cuprates are commonly described by a three-band Emery-like model with strong pd hybridization [16], the generic microscopic many-particle description for the electronic line shapes of pure and hole-doped infinite-layer nickelates is still lacking. Here, based on extant experimental [17–19] and theoretical [4–10] studies we argue that, in contrast to cuprates, the NdNiO$_2$ system is a MO superconductor

closely related to phase-separated K$_x$Fe$_2$Se$_2$ [20], exhibiting orbital-selective low-energy electronic excitations. This is partially motivated by the intrinsically metastable phase of infinite-layer nickelates, showing the presence of unreduced forms of NdNiO$_3$ perovskite structure [21] in different regions (see our discussion below), as in Fe-chalcogenide superconductors [20,22].

The infinite-layer nickelate thin films are stabilized by soft-chemistry topotactic reduction [13,23] of the perovskite phase, grown epitaxially on SrTiO$_3$ (001) substrates and capped with a thin layer of SrTiO$_3$ by pulsed laser deposition [24,25]. Importantly, the possibility of hydrogen incorporation has been found, for example, in topotactically reduced NdNiO$_3$ films [26], showing an oxyhydride NdNiO$_{3-x}$H$_y$ phase with a defect-fluorite structure in the surface region. Topotactic hydrogens are usually found in SrTiO$_3$ thin films commonly used as substrate and capping layer for infinite-layer nickelate films, providing an additional route for hole doping via hydrogenation in this material class [27].

Using density functional theory (DFT) calculations, Ref. [28] found that the existence of H atoms from the chemical reduction reaction might be vital to stabilize the NdNiO$_2$ phase via the formation of a hydride compound NdNiO$_2$H, which in turn may explain the absence of superconductivity in Sr-doped NdNiO$_2$ films without chemical reduction, providing relevant insights on the role played by the coexistence of multiple phases in this material class. Additional evidence of phase coexistence is provided by locally resolved electron energy loss spectroscopy (EELS) [21], revealing distinct O-K near-edge fine structures in different regions of the same sample, including some crystalline defects and small pockets of incomplete reduction of pristine perovskite to tetragonal NdNiO$_2$. Thus, due to decomposition into competing phases [13] as well as the formation of one-dimensional hydrogen

chains [28,29] a fine-tuning of experimental reduction conditions is needed [25]. However, since the presence of some unreduced perovskite regions is likely to be unavoidable in extant experiments [21], local variations of hydrogen concentration or the presence of unreduced perovskite might result in the coexistence of superconducting and nonsuperconducting phases. These competing phases are expected to mask the electronic character of the pure superconducting 112 phase as in the $K_x Fe_2 Se_2$ superconductor. Motivated thereby, in this work we explore the correlated electronic structure reconstruction of pure and hole-rich $NdNiO_2$, providing a description of the elusive valence states [30] probed by resonant inelastic x-ray scattering (RIXS) [17], based on the coexistence of long-lived metastable phases [28] with distinct low- and high-energy electronic excitations.

Similar to $K_x Fe_{2-y} Se_2$ systems [31], here we adopt a Mottness view with incorporation of sizable five-orbital correlations in the Ni-$3d$ shell of infinite-layer $NdNiO_2$. As shown below, phase coexistence based on a correlated five-orbital problem satisfactorily resolves the electronic state probed by RIXS at the Ni-L_3 edge (a core level $2p$ to valence $3d$ transition) [17], showing the coexistence of pure $3d^9$ and $3d^8$ hole-rich phases in the real solid.

Starting with the d^9 parent compound, where $NdNiO_2$ is close to Mott localization, sizable electronic correlations promotes new physical effects upon doping. Correlation can induce changes in orbital polarization [32,33] naturally yielding coexistent metallic, insulating, and bad-metallic states. To correctly describe these states, in this work, we employ the dynamic treatment of local correlation in the form of density functional plus dynamical mean-field theory (DFT+DMFT) [34]. Our results allow us to discuss the influence of orbital-selective electronic structure reconstruction in the five orbital problem of $NdNiO_2$ and follow this up with specific predictions which can be tested in future experiments.

II. THEORY AND RESULTS

The electronic properties of infinite-layer nickelates are knowingly governed by the interplay between the on-site electron-electron interactions and MO degrees of freedom [5–10]. Similar to Fe-based superconductors, the one-electron Hamiltonian considered here to infinite-layer $NdNiO_2$ is $H_0 = \sum_{\mathbf{k},a,\sigma} \epsilon_a(\mathbf{k}) c^\dagger_{\mathbf{k},a,\sigma} c_{\mathbf{k},a,\sigma}$, where $a = xy, xz, yz, x^2 - y^2, 3z^2 - r^2$ denotes its Ni-$3d$ orbitals and $\epsilon_a(\mathbf{k})$ is the corresponding band dispersion, which encodes details of the one-electron band structure [6,8–10]. Here, we work in the local basis which diagonalizes the one-particle density matrix; see our discussion below. In this basis residual interorbital one-electron overlap is zero, and so in the paramagnetic phase the many-particle Green's functions and self-energies become diagonal in orbital and spin flavor [35]. These five orbitals are the relevant one-particle inputs for MO DFT+DMFT, which generates a reconstructed electronic state with reduced orbital polarization, as shown below. Similar to Fe-based superconductors [31] the correlated many-body Hamiltonian relevant for the normal state of $NdNiO_2$ superconductor reads $H_{int} = U \sum_{i,a} n_{i,a,\uparrow} n_{i,a,\downarrow} + U' \sum_{i,a \neq b} n_{i,a} n_{i,b} - J_H \sum_{i,a \neq b} \mathbf{S}_{i,a} \cdot \mathbf{S}_{i,b}$, where U and $U' = U - 2J_H$ are intra-

and interorbital Coulomb interaction terms and J_H denotes the Hund's coupling.

We evaluate the many-particle Green's functions $[G_{a,\sigma}(\omega)]$ of the five-orbital Hamiltonian $H = H_0 + H_{int}$ using the MO iterated perturbation theory (MO-IPT) as impurity solver [36]. This interpolative ansatz is known to account for the correct low- and high-energy behavior of the one-particle spectral function Hubbard-like models in the large-dimensional limit (DMFT). It ensures the Mott-Hubbard metal-insulator transition from a correlated FL metal to a Mott insulator as a function of the Coulomb interaction U. The MO-IPT scheme is computationally very efficient, with real frequency output at zero and finite temperatures, and it gives results in qualitative accord with continuous-time quantum Monte Carlo (CT-QMC) calculations for real MO systems [22,37].

Bloch electronic states were calculated using density functional theory in the local density approximation (Perdew-Zunger), using standard solid state pseudopotentials available from the ps library v1.0.0 [38]. The plane-wave expansion of valence electron wave functions and charge density used kinetic energy cutoffs of 80 and 800 Ry, respectively. Calculations were performed using the pw.x code (v6.7) of the Quantum Espresso (QE) package, based on experimental crystal data [39]. SCF calculations were run on a k grid of $11 \times 11 \times 11$ data points.

Analogously to our earlier calculations for $BaFe_2Se_3$ [40], we have chosen a projection local basis in which the Ni-$3d$ occupancy matrix is diagonal. Due to strong hybridization of O-$2p$ with Nd-$5d$ orbitals and Ni-$3d$ orbitals, the number of bands considered for the DFT calculation of the occupation matrix and therefore the projection band energy range are critical factors. A tight-binding band structure model was obtained from interpolating maximally localized Wannier functions (MLWFs), calculated with the Wannier90 package [41] (v3.0). As initial guess for Wannier functions, $2p$ and $3d$ orbitals were used for O and Ni, respectively, and just $5d_{z^2}$ for Nd (12 MLWFs in total). Iterative spread minimization provided real-valued MLWFs using a $1.0 \times 10^{-12}\Omega$ convergence tolerance. 15 Bloch states were considered, after exclusions of 6 lower-lying states (outer energy window maximum 20.80 eV). An inner, frozen energy window in the range 7.3–13.95 eV was used to disentangle 12 states for Wannierization. The choice of those energy ranges guarantees Ni-localized, atomic-like Wannier functions, with the correct site symmetry and intersite symmetry equivalence. Similar to Ref. [40], this provides a robust strategy for the choice of an atomic-like basis in a situation of strong interband hybridization in the real solid. The corresponding projected DOSs are shown in Fig. 1.

We first discuss our DFT results. In Fig. 1 we display the orbital-resolved spectral functions of $NdNiO_2$ obtained as described above. Consistent with earlier studies [10,19] the D_{4h} tetragonal symmetry of infinite-layer $NdNiO_2$ lifts the degeneracy of the Ni-$3d$ orbitals such that $3z^2 - r^2$ becomes the ground state orbital, followed by $yz, xz, xy, x^2 - y^2$ orbitals, respectively. Similar to Fe-based superconductors double degeneracy is found within the yz, xz orbital sector, a characteristic akin to the D_{4h} crystal-field splitting. However in contrast to the $3d^6$ Fe-based superconductors, strong orbital polarization is found in the $3d^9$ nominal state of infinite-layer
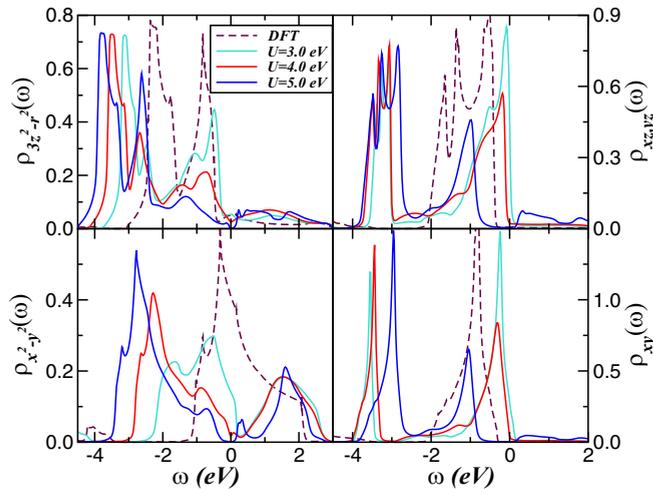
FIG. 1. Ni-$3d$ DFT and DFT+DMFT spectral functions of NdNiO$_2$, showing the evolution of the correlated spectra for three different U values and fixed $J_H = 0.7$ eV. Notice the electronic reconstruction due to sizable multiorbital correlations and the downshift of the polarized in DFT $3z^2 - r^2$, xz, yz, xy orbitals as well as the emergence of all-orbital Mott localization at $U = 5.0$ eV.

Ni superconductors. As seen in Fig. 1, apart from the nearly half-filled $x^2 - y^2$ orbital, the other orbitals are close to fully occupied, with the top of the valence band laying slightly below the Fermi level, $E_F = \omega = 0$. A small deviation from this full orbital polarization fingerprint is seen within the $3z^2 - r^2$ orbital, where residual electronic states are found above E_F due to finite hybridization of this orbital sector with Nd-$5d$ conduction electrons [42]. Among the five Ni-$3d$ orbitals, the t_{2g} shell of NdNiO$_2$ is fully occupied, being less relevant to the electronic states at E_F within the nominal $3d^9$ state [8]. Additionally, while the $3z^2 - r^2$ spectral function shows nearly one-dimensional orbital character with sharp peaks at 2.3 and 0.73 eV binding energy, the $x^2 - y^2$ and xy channels display two-dimensional-like band dispersion with clear particle-hole asymmetry. Finally, due to interband mixing at one-particle level the xz, yz bare electronic state shows combined one- and two-dimensional electronic features responsible for the three-peak structure in the orbital-resolved one-particle density of states (DOS) of Fig. 1. How these orbital-selective DFT spectral functions of NdNiO$_2$ are reshaped by dynamical correlations and hole doping is our focus below.

We next discuss the correlated electronic reconstruction of the Ni-$3d$ states. In Fig. 1 we present our DFT+DMFT results obtained for three different U values and fixed $J_H = 0.7$ eV in the $3d^9$ nominal state. As seen, at $U = 3.0$ eV the shape of the $x^2 - y^2$ DFT DOS is strongly renormalized, displaying emergent lower and upper Hubbard bands at approximately ± 1.6 eV. Similar to Ref. [7] the spectral functions of the low-lying orbitals are pushed up in energy, while the $x^2 - y^2$ orbital is dynamically shifted to low energy and becomes more populated. Particularly interesting in our DFT+DMFT results for $U = 3.0$ eV is the emergence of low-energy Kondo-quasiparticle resonances near E_F in the partially depopulated $3z^2 - r^2$, xz, yz, xy orbitals due to strong interorbital proximity effect induced by U', a

fingerprint of correlated semiconductors [43]. Additionally, with increasing U, the low-energy coherence characteristic of Kondo quasiparticles is lost, with spectral weight being transferred to higher energies with the concomitant enhancement of spectral weight of the incoherent Hubbard bands [3], as seen in our results for $U = 4.0$ eV. Finally, at $U = 5.0$ eV the NdNiO$_2$ parent compound is in the Mott side of the correlated phase diagram [44], with a Mott-Hubbard gap emerging across E_F on all orbitals.

The appearance of Kondo correlations in the populated low-lying orbitals remains rather counterintuitive since they are almost fully occupied in the bare, one-band picture. Normally, for the one-band Hubbard model electrons are known to be weakly correlated in systems far from half filling [3,44]. This canonical understanding, however, does not hold completely true for MO systems with sizable interorbital correlations [45]. As shown in Fig. 1 the effective band filling combined with MO Hartree shifts leads to electron flow from populated orbitals to the half-filled one. This effect is similar to that reported for spin-polarized ferromagnetic systems, where the valence band DOS of the majority spin channel is shifted toward E_F [45] with the less polarized channel being barely affected by electron-electron interactions [45,46]. Also relevant to NdNiO$_2$ is the presence of the van Hove singular peaks in the semiconducting channels which are dynamically shifted toward E_F at finite U values. This in turn enhances intrinsic electron-electron interactions in NdNiO$_2$, driving the system toward Mott localization with a clear Mott-Hubbard gap emerging on all orbitals at $U = 5.0$ eV in Fig. 1. Here, the interplay between orbital depolarization [33] and sizable intra- and interorbital Coulomb correlations give rise to an extended van Hove singularity regime with similarities akin to that discussed, for example, for doped graphene [47] and Sr$_2$RuO$_4$ [48]. For the sake of clarity, we shall notice here that in low-dimensional systems the bare one-particle spectral function usually diverges and the excess of charge carriers enhances intrinsic electronic correlations [49], an effect which is now commonly referred to as extended van Hove singularity [47]. Taken together, our results in Fig. 1 suggests that strong electronic correlations in the NdNiO$_2$ parent compound result from the interplay between orbital depolarization and the proximity of the van Hove singularities to E_F. This is the key step, which allows us to understand the electronic reconstruction in this system.

To better understand the role played by interorbital proximity effect induced by U' and J_H, in Fig. 2 we show the evolution of the orbital occupancies $n_{a,\sigma}$ (upper panel) and the renormalized orbital splittings δ_a (lower panel) as a function of the on-site Coulomb interaction U. As seen, DFT+DMFT severely renormalizes the center of gravity δ_a of each Ni-$3d$ band as well as the orbital occupancies $n_{a,\sigma}$, promoting reduced orbital polarization [33]. Also interesting is the emergent orbital switching between the xz, yz, and xy orbitals, as seen in the upper panel of Fig. 2. This fact, generic to MO systems, is an interesting manifestation of correlation-induced orbital rearrangement, which might control structural changes across the pressure-induced Mott transition [50] in NdNiO$_2$ and analogs.

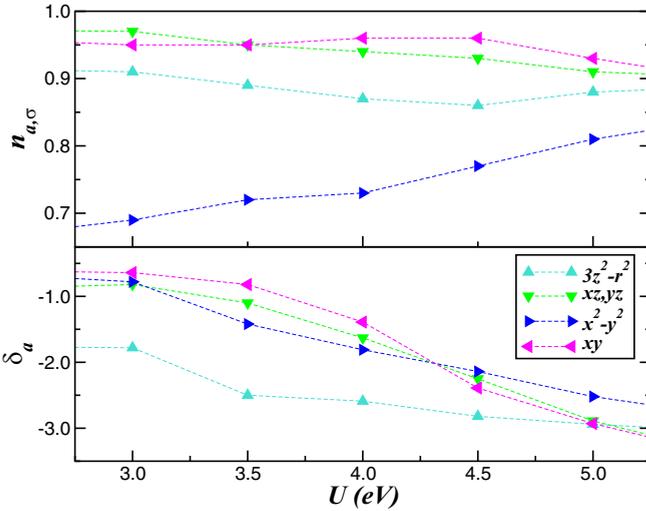To get additional insights into the normal state electronic structure reconstruction of bulk NdNiO$_2$, we now focus on

FIG. 2. Evolution of the DFT+DMFT results for the orbital occupations n_σ^a (upper panel) and the renormalized orbital splittings δ_a (lower panel) as function of the on-site Coulomb interaction U. Notice the switching in the orbital occupancies between the xz, yz, and xy orbitals at $U = 3.5$ eV, a behavior characteristic of orbital-selective Mottness. An additional feature to be seen is the reduction of orbital polarization with increasing U.

FIG. 3. Electronic reconstruction on the Ni-$3d$ spectral functions of NdNiO$_2$ computed using $U = 4.0$ eV for the stoichiometric $n = 9.0$ to the hole-rich regime $n = 8.0$. Particular features to be seen are the large spectral weigh transfer and the orbital differentiation with coexisting pseudogapped and Kondo-like features at low energies upon changes in the total band filling n.

the effect of hole-doping the parent compound. Even though experimental data exist [1], the appearance of novel electronic states in a wide variety of other correlated electron systems makes this an important question of general scope. Our aim here is to build upon the strengths of correlated electronic structure modeling to introduce dynamical spectral weigh transfer (SWT) via hole doping within a range relevant to experiments [17,18]. As seen in Fig. 3, our results for fixed $U = 4.0$ eV and $J_H = 0.7$ eV confirm that metallicity is enhanced upon hole-doping an orbital-selective Kondo-pseudogapped parent compound. This is tied to the fact that the Kondo-quasiparticle resonance of the xz, yx, xy orbitals is shifted toward E_F upon doping as well as the partial suppression of the pseudogap feature in the $3z^2 - r^2$ orbital at low energies. An intriguing observation, however, is the robustness of the pseudogapped line shape in the $x^2 - y^2$ orbital sector in spite of the intrinsic orbital-selective metallization in the hole-rich ($n \approx 8.0$) regime of NdNiO$_2$. What is the origin of the orbital-selective features seem in Fig. 3? In correlated MO systems like NdNiO$_2$, scattering between different carriers in orbital states leads to two main effects: an orbital-dependent shift of the $3d$ bands relative to each other via static-Hartree contributions and strong dynamical correlations due to sizable U, U', and J_H cause appreciable SWT over large energy scales upon carrier doping. Thus, in the hole-rich regime coexisting Kondo-quasiparticle and pseudogap components with distinct electronic line shape should be visible at low energies, in spite of large-scale SWT induced by dynamical electron-electron interactions.

We now compare our DFT+DMFT(MO-IPT) calculation with published experimental results [17], showing the possibility of intrinsic phase coexistence in the real solid. The hydrogenated system has lattice constants similar to those of the pure form, leading to comparable x-ray diffraction patterns
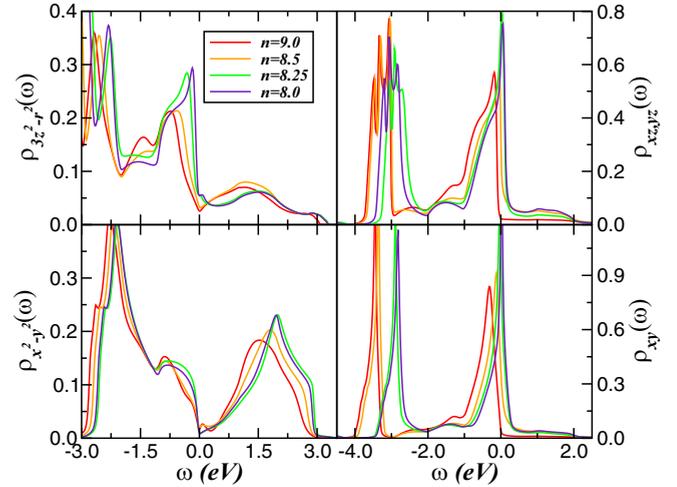
[28]. To compute the correlated spectral functions of hole-rich NdNiO$_2$ we therefore used the DFT results of Fig. 1 to derive the electronic reconstruction induced by hole-doping the parent compound.

In Fig. 4 our DFT+DMFT results are compared with experimental RIXS data of Ref. [17]. After the intensity being normalized to coincide with theory, good qualitative agreement is observed up to 0.65 eV binding energy. Particularly interesting is the peak-dip-hump feature seen in experiment, which is well reproduced by theory. This includes the width of the quasiparticle resonance near E_F and the shoulder feature at 0.6 eV binding energy. It is worth noting here that total spectra in the main panel of Fig. 4 are obtained assuming a coexisting phase scenario composed of nominal $3d^9$ and hole-rich $3d^8$ electronic states. Within this scenario, we find qualitative agreement with experiment by averaging the total spectral function ($\rho_{total} = \rho_{total}^{3d^9} + \rho_{total}^{3d^8}$) of the different total electronic states using the ratio $3d^9$: 25% and $3d^8$: 75%. As observed in the inset of Fig. 4, the low-energy component of the one-particle spectra has a large $3d^8$ contribution of the orbital-selective metal, while the shoulder feature at 0.6 eV below E_F is mostly related to the occupied $3d^9$ spectral function, which is Mott localized at $U = 4.6$ eV. Although the intensity of the experimental data is sensitive to the partial contributions, our theory-experiment comparison suggest an averaged electronic state composed of Mott-localized $3d^9$, in contrast with charge-transfer insulating state characteristic of cuprates superconductors [44], and itinerant $3d^8$ electronic states in the real crystal. Interestingly, our theory-experiment comparison suggests that the infinite-layer NdNiO$_2$ system separates into two phases similar to the K$_x$Fe$_2$Se$_2$ superconductor [31], which contains a minor superconducting phase and a major nonsuperconducting Mott-localized phase. Beyond the scenario of spatial phase separation in the normal state with slightly different coupling parameters [51] more
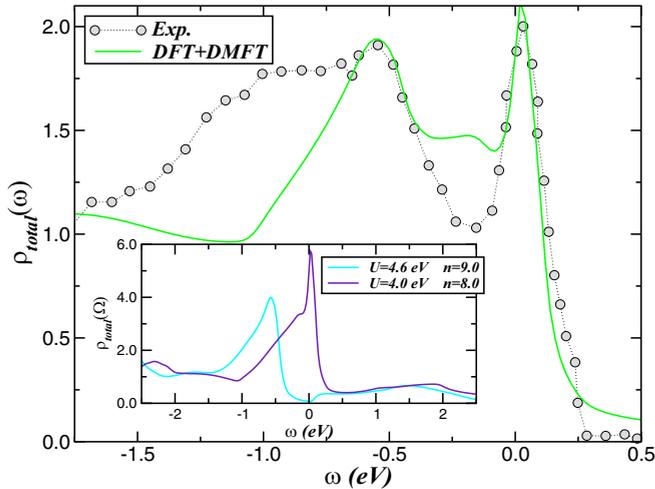
FIG. 4. Theory-experiment comparison between the total DFT+DMFT spectral function of phase-separated $NdNiO_2$ and resonant inelastic x-ray scattering (RIXS) data taken from Ref. [17], showing qualitative good agreement. A particularly interesting feature is the peak-dip-hump in experiment at energies up to -0.6 eV, which is well accounted for by the total DFT+DMFT spectra multiplied by the Fermi function. Notice the low-energy Kondo-quasiparticle resonance which nicely agrees with experiment. Inset shows the total density of states for the stoichiometric ($n = 9.0$) and hole-rich ($n = 8.0$) $NdNiO_2$ used to compute the total DFT+DMFT spectral function of the mixed phase shown in the main panel.

experimental and theoretical work is needed to decide whether this coexisting scenario can also explain the doping dependence of the one-particle spectral function of the Sr-doped $NdNiO_2$ superconductor [21,52].

In Fig. 5 we show the changes induced by the interplay between total electron band filling and Coulomb (intra- and interorbital) correlation effects. As already shown in the inset
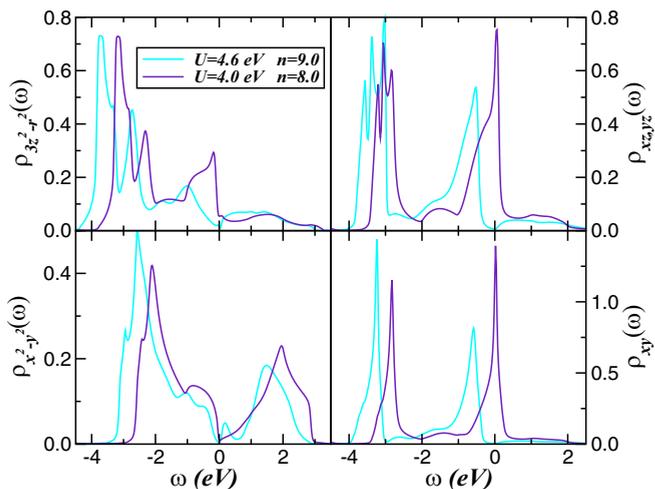

FIG. 5. DFT+DMFT spectral functions of undoped ($n = 9.0$) and hole-rich ($n = 8.0$) $NdNiO_2$, showing the changes in the correlated spectra for two U values and fixed $J_H = 0.7$ eV. Notice the electronic localization at $U = 4.6$ eV and the orbital-selective metal at $U = 4.0$ eV.

of Fig. 4 at $U = 4.6$ eV stoichiometric $NdNiO_2$ is a Mott insulator, however, with different degree of electronic localization, as seen in Fig. 5. On the other hand, at $U = 4.0$ eV an orbital-selective metal is predicted to exist in hole-rich $NdNiO_2$. In our formalism this correlated electronic state can be taken as a manifestation of metallic screening [53], where U and U' are renormalized as compared to their values in the insulating phase [54]. Interestingly, due to its nearly half-filled nature the $x^2 - y^2$ orbital remains Mott localized while the $xz, yz, xy, 3z^2 - r^2$ are metallic. Thus, our results in Fig. 5 suggest that the charge carriers in hole-rich $NdNiO_2$ have a dual nature, where effectively Mott-localized states coexist with itinerant electronic states. In this two-fluid scenario selective Mott localization of $x^2 - y^2$ states implies that this orbital now act like an intrinsic source of electronic disorder in the system [50]. With $n = 8.0$, for example, this suggests that an intrinsic disorder potential, arising from orbital-selective physics might exist in hole-rich $NdNiO_2$. Such behavior results from strong scattering between effectively (Mott) localized and itinerant components of the full DMFT matrix propagators. This behavior is intimately linked to orbital-selective Mott-like physics within DMFT [55].

Our direct theory-experiment comparison in Fig. 4 provides a natural explanation for the metallic bulk state of $NdNiO_2$ seen in extant RIXS experiments [17,18]. The DFT+DMFT $3d^9/3d^8$ Mott/metal electronic state shown in this figure correctly describes the two-peak electronic structure with a zero-energy Kondo-quasiparticle resonance and the shoulder feature at -0.6 eV as seen experimentally. The situation here is similar to that reported, for example, for the $1T$-$TaSe_2$ crystal, which shows a multitude of correlated states at a surface composed of metallic and Mott-localized subsystems [51]. Although our modeling qualitatively captures extant RIXS observations at low binding energies, it requires as described above slightly different U values for the Mott/metal subsystems as well as an effective combination of nonfluctuating $3d^8$ and $3d^9$ valence states. This suggests the existence of a quenched MO mixed-valent state, which is fundamentally different from the effective single-band model of cuprate superconductors as correctly pointed out in Ref. [21]. However, given the uncertainty regarding the boundary between the different phases, particularly upon electron doping via hydrogenation [28,29], a more realistic model is needed to better account for the microscopic details of the nonfluctuating mixed-valent system. Particularly, the different coupling strengths between the Mott/metal subsystems [51] due to mesoscale pattern formation [56] might open a link between $NdNiO_2$ and $K_x Fe_{2-y} Se_2$ films [20], both exhibiting Mott-localized and unconventional superconducting phases.

III. CONCLUSION

To summarize, we have used DFT+DMFT for the five-orbital model to derive a correlation-induced electronic reconstruction in the normal state of the $NdNiO_2$ superconductor. We have shown that orbital selectivity with coexisting pseudogapped and coherent electronic states and the proximity to Mottness characterize the paramagnetic normal state of undoped $NdNiO_2$ infinite-layer superconductor. Good qualitative agreement with extant experimental RIXS data [17]

within a single theoretical picture lends support to our proposal. The emergence of Mott/metal phase coexistence with different nominal valence should be considered as a multiorbital manifestation of slightly quenching electron-electron interactions via hole overdoping an orbital-selective Mott insulator. Decreasing intrinsic orbital polarization upon hole-doping the NdNiO$_2$ parent compound suggests a promising and practical route to access two-fluid orbital differentiation, where the $x^2 - y^2$ channel retains its intrinsic pseudogapped electronic nature while the xz, yz, xy density of states sharpens at low temperatures and dominates the low-energy spectral function of hole-rich NdNiO$_2$ in good qualitative accord with RIXS data [17,18]. This behavior is consistent with the appearance of a domain-dependent mixed-valent metal [21] of coexisting heavy Fermi liquid and Mott-localized electronic states. The identification of emergent mesoscale phase separation in NdNiO$_2$ promises the discovery of a rich variety of nonlocal phenomena in modulation-doped Mott insulators [57], some of which even with coexisting Mott-insulating, pseudogapped, and superconducting quantum matter phases within the same crystal structure.

ACKNOWLEDGMENTS

[1] Y. Ji, J. Liu, L. Li, and Z. Liao, J. Appl. Phys. **130**, 060901 (2021); Y. Nomura and R. Arita, Rep. Prog. Phys. **85**, 052501 (2022); X. Zhou, P. Qin, Z. Feng, H. Yan, X. Wang, H. Chen, Z. Meng, and Z. Liu, Mater. Today **55**, 170 (2022); Q. Gu and H.-H. Wen, The Innovation **3**, 100202 (2022); see also K. Lee, B. Y. Wang, M. Osada, B. H. Goodge, T. C. Wang, Y. Lee, S. Harvey, W. J. Kim, Y. Yu, C. Murthy, S. Raghu, L. F. Kourkoutis, and H. Y. Hwang, arXiv:2203.02580.

[2] H. Chen, A. Hampel, J. Karp, Frank Lechermann, and A. J. Millis, Front. Phys. **10**, 835942 (2022).

[3] A. Georges, G. Kotliar, W. Krauth, and M. J. Rozenberg, Rev. Mod. Phys. **68**, 13 (1996).

[4] F. Lechermann, Phys. Rev. B **101**, 081110(R) (2020).

[5] J. Karp, A. Hampel, and A. J. Millis, Phys. Rev. B **103**, 195101 (2021).

[6] A. S. Botana and M. R. Norman, Phys. Rev. X **10**, 011024 (2020).

[7] P. Worm, L. Si, M. Kitatani, R. Arita, J. M. Tomczak, and K. Held, Phys. Rev. Mater. **6**, L091801 (2022).

[8] Z. Liu, C. Xu, C. Cao, W. Zhu, Z. F. Wang, and J. Yang, Phys. Rev. B **103**, 045103 (2021).

[9] Y. Wang, C.-J. Kang, H. Miao, and G. Kotliar, Phys. Rev. B **102**, 161118(R) (2020).

[10] T. Y. Xie, Z. Liu, Chao Cao, Z. F. Wang, J. L. Yang, and W. Zhu, Phys. Rev. B **106**, 035111 (2022).

[11] L. Craco, A. S. de Arruda, and S. Leoni, Phys. Rev. Res. **4**, 043036 (2022).

[12] V. I. Anisimov, D. Bukhvalov, and T. M. Rice, Phys. Rev. B **59**, 7901 (1999).

[13] M. A. Hayward, M. A. Green, M. J. Rosseinsky, and J. Sloan, J. Am. Chem. Soc. **121**, 8843 (1999); see also M. Crespin, P. Levitz, and L. Gatineau, J. Chem. Soc., Faraday Trans. 2 **79**, 1181 (1983).

[14] K. W. Lee and W. E. Pickett, Phys. Rev. B **70**, 165109 (2004).

[15] D. Zhao, Y. B. Zhou, Y. Fu, L. Wang, X. F. Zhou, H. Cheng, J. Li, D. W. Song, S. J. Li, B. L. Kang, L. X. Zheng, L. P. Nie, Z. M. Wu, M. Shan, F. H. Yu, J. J. Ying, S. M. Wang, J. W. Mei, T. Wu, and X. H. Chen, Phys. Rev. Lett. **126**, 197001 (2021).

[16] L. Craco, Phys. Rev. B **79**, 085123 (2009).

[17] M. Hepting, D. Li, C. J. Jia, H. Lu, E. Paris, Y. Tseng, X. Feng, M. Osada, E. Been, Y. Hikita, Y. D. Chuang, Z. Hussain, K. J. Zhou, A. Nag, M. Garcia-Fernandez, M. Rossi, H. Y. Huang, D. J. Huang, Z. X. Shen, T. Schmitt *et al.*, Nat. Mater. **19**, 381 (2020).

[18] G. Krieger, L. Martinelli, S. Zeng, L. E. Chow, K. Kummer, R. Arpaia, M. Moretti Sala, N. B. Brookes, A. Ariando, N. Viart, M. Salluzzo, G. Ghiringhelli, and D. Preziosi, Phys. Rev. Lett. **129**, 027002 (2022).

[19] M. Rossi, H. Lu, A. Nag, D. Li, M. Osada, K. Lee, B. Y. Wang, S. Agrestini, M. Garcia-Fernandez, J. J. Kas, Y.-D. Chuang, Z. X. Shen, H. Y. Hwang, B. Moritz, Ke-Jin Zhou, T. P. Devereaux, and W. S. Lee, Phys. Rev. B **104**, L220505 (2021).

[20] W. Li, H. Ding, P. Deng, K. Chang, C. Song, K. He, L. Wang, X. Ma, J.-P. Hu, X. Chen, and Q.-K. Xue, Nat. Phys. **8**, 126 (2012).

[21] B. H. Goodge, D. Li, K. Lee, M. Osada, B. Y. Wang, G. A. Sawatzky, H. Y. Hwang, and L. F. Kourkoutis, Proc. Natl. Acad. Sci. USA **118**, e2007683118 (2021).

[22] L. Craco and S. Leoni, Phys. Rev. B **100**, 121101(R) (2019).

[23] P. Puphal, B. Wehinger, J. Nuss, K. Küster, U. Starke, G. Garbarino, B. Keimer, M. Isobe, and M. Hepting, Phys. Rev. Mater. **7**, 014804 (2023).

[24] D. Li, K. Lee, B. Y. Wang, M. Osada, S. Crossley, H. R. Lee, Y. Cui, Y. Hikita, and H. Y. Hwang, Nature (London) **572**, 624 (2019).

[25] K. Lee, B. H. Goodge, D. Li, M. Osada, B. Y. Wang, Y. Cui, L. F. Kourkoutis, and H. Y. Hwang, APL Mater. **8**, 041107 (2020).

[26] T. Onozuka, A. Chikamatsu, T. Katayama, T. Fukumura, and T. Hasegawa, Dalton Trans. **45**, 12114 (2016).

[27] P. Puphal, V. Pomjakushin, R. A. Ortiz, S. Hammoud, M. Isobe, B. Keimer, and M. Hepting, Front. Phys. **10**, 842578 (2021).

[28] O. I. Malyi, J. Varignon, and A. Zunger, Phys. Rev. B **105**, 014106 (2022).

[29] L. Si, P. Worm, D. Chen, and K. Held, Phys. Rev. B **107**, 165116 (2023).

[30] L. J. P. Ament, M. van Veenendaal, T. Devereaux, J. Hill, and J. van den Brink, Rev. Mod. Phys. **83**, 705 (2011).

[31] L. Craco, M. S. Laad, and S. Leoni, Phys. Rev. B **84**, 224520 (2011); L. Craco and S. Leoni, Europhys. Lett. **136**, 27002 (2021).

[32] P. Werner and A. J. Millis, Phys. Rev. Lett. **99**, 126405 (2007); Y. Ni, Y.-M. Quan, J. Liu, Y. Song, and L.-J. Zou, Phys. Rev. B **103**, 214510 (2021).

[33] A. Liebsch, Phys. Rev. B **77**, 115115 (2008).

[34] G. Kotliar, S. Y. Savrasov, K. Haule, V. S. Oudovenko, O. Parcollet, and C. A. Marianetti, Rev. Mod. Phys. **78**, 865 (2006).

[35] L. Craco, M. S. Laad, S. Leoni, and E. Müller-Hartmann, Phys. Rev. B **70**, 195116 (2004).

[36] L. Craco, Phys. Rev. B **77**, 125122 (2008).

[37] L. Craco and S. Leoni, Phys. Rev. B **102**, 045142 (2020).

[38] A. Dal Corso, Comput. Mater. Sci. **95**, 337 (2014).

[39] M. A. Hayward and M. J. Rosseinsky, Solid State Sci. **5**, 839 (2003).

[40] L. Craco and S. Leoni, Phys. Rev. B **101**, 245133 (2020).

[41] G. Pizzi *et al.*, J. Phys.: Condens. Matter **32**, 165902 (2020).

[42] G.-M. Zhang, Y.-F. Yang, and F.-C. Zhang, Phys. Rev. B **101**, 020501(R) (2020).

[43] M. Arita, K. Shimada, Y. Takeda, M. Nakatake, H. Namatame, M. Taniguchi, H. Negishi, T. Oguchi, T. Saitoh, A. Fujimori, and T. Kanomata, Phys. Rev. B **77**, 205117 (2008); see also A. Bentien, S. Johnsen, G. K. H. Madsen, B. B. Iversen, and F. Steglich, Europhys. Lett. **80**, 17008 (2007).

[44] M. Imada, A. Fujimori, and Y. Tokura, Rev. Mod. Phys. **70**, 1039 (1998).

[45] A. Droghetti, M. M. Radonjić, A. Halder, I. Rungger, and L. Chioncel, Phys. Rev. B **105**, 115129 (2022).

[46] J. Faúndez, T. N. Jorge, and L. Craco, Phys. Rev. B **97**, 115149 (2018).

[47] J. L. McChesney, A. Bostwick, T. Ohta, T. Seyller, K. Horn, J. González, and E. Rotenberg, Phys. Rev. Lett. **104**, 136803 (2010).

[48] A. Liebsch and A. Lichtenstein, Phys. Rev. Lett. **84**, 1591 (2000).

[49] S. Link, S. Forti, A. Stöhr, K. Küster, M. Rösner, D. Hirschmeier, C. Chen, J. Avila, M. C. Asensio, A. A. Zakharov, T. O. Wehling, A. I. Lichtenstein, M. I. Katsnelson, and U. Starke, Phys. Rev. B **100**, 121407(R) (2019); P. Rosenzweig, H. Karakachian, D. Marchenko, K. Küster, and U. Starke, Phys. Rev. Lett. **125**, 176403 (2020).

[50] L. Craco, M. S. Laad, and S. Leoni, Sci. Rep. **7**, 2632 (2017).

[51] Y. Chen, W. Ruan, J. D. Cain, R. L. Lee, S. Kahn, C. Jia, A. Zettl, and M. F. Crommie, Phys. Rev. B **106**, 075153 (2022).

[52] A. Kreisel, B. M. Andersen, A. T. Romer, I. M. Eremin, and F. Lechermann, Phys. Rev. Lett. **129**, 077002 (2022).

[53] Y. Nomura, M. Hirayama, T. Tadano, Y. Yoshimoto, K. Nakamura, and R. Arita, Phys. Rev. B **100**, 205138 (2019); F. Petocchi, V. Christiansson, F. Nilsson, F. Aryasetiawan, and P. Werner, Phys. Rev. X **10**, 041047 (2020); F. Lechermann, Phys. Rev. Mater. **5**, 044803 (2021).

[54] M. S. Laad, L. Craco, and E. Müller-Hartmann, Phys. Rev. B **73**, 045109 (2006).

[55] S. Biermann, L. de' Medici, and A. Georges, Phys. Rev. Lett. **95**, 206401 (2005).

[56] See A. Wendl, H. Eisenlohr, F. Rucker, C. Duvinage, M. Kleinhans, M. Vojta, and C. Pfleiderer, Nature (London) **609**, 65 (2022).

[57] F. Ming, D. Mulugeta, W. Tu, T. S. Smith, P. Vilmercati, G. Lee, Y.-T. Huang, R. D. Diehl, P. C. Snijders, and H. H. Weitering, Nat. Commun. **8**, 14721 (2017); see also Y.-L. Xiong, J.-Q. Guan, R.-F. Wang, C.-L. Song, X.-C. Ma, and Q.-K. Xue, Chin. Phys. B **31**, 067401 (2022).